



Chemistry A European Journal

 **Chemistry
Europe**
European Chemical
Societies Publishing

Accepted Article

Title: Triarylborane Appended Anils and Boranils: Solid State Emission, Mechanofluorochromism and Phosphorescence

Authors: Pakkirisamy Thilagar, Rajendra Prasad Nandi, Pagidi Sudhakar, and Neena K Kalluvettukuzhy

This manuscript has been accepted after peer review and appears as an Accepted Article online prior to editing, proofing, and formal publication of the final Version of Record (VoR). This work is currently citable by using the Digital Object Identifier (DOI) given below. The VoR will be published online in Early View as soon as possible and may be different to this Accepted Article as a result of editing. Readers should obtain the VoR from the journal website shown below when it is published to ensure accuracy of information. The authors are responsible for the content of this Accepted Article.

To be cited as: *Chem. Eur. J.* 10.1002/chem.202001470

Link to VoR: <https://doi.org/10.1002/chem.202001470>

WILEY-VCH

Triarylborane Appended Anils and Boranils: Solid State Emission, Mechanofluorochromism and Phosphorescence

Rajendra Prasad Nandi, Pagidi Sudhakar, Neena K. Kalluvettukuzhy and Pakkirisamy Thilagar*

Rajendra Prasad Nandi, Dr. Sudhakar Pagidi, Dr. Neena K. Kalluvettukuzhy and Prof. Pakkirisamy Thilagar
Department of Inorganic and Physical Chemistry, Indian Institute of Science, Bangalore-560012, India
E-mail: thilagar@iisc.ac.in

Supporting information for this article is given via a link at the end of the document.

Abstract: Herein we report the design, synthesis, optical and mechanoluminescence properties of a series of conjugates having covalently linked triarylborane (TAB) and anil/boranil (TAB-anil: **1a-3a** and TAB-boranil: **1-3**). The electronic interaction between TAB and anil/boranil in **1a-3a** and **1-3** were finetuned by changing the position of the boryl moiety on the phenyl spacer connecting -BMe₂ (Mes = mesityly) and anils/boranils units. Boryl moiety at the *meta* position (**1a**) of the phenyl spacer stabilizes enolic form (E-OH) while boryl moiety at the *para* position (**2a** and **3a**) stabilize the keto form (Z-NH) in the solid state. However, in solutions **1a**, **2a** and **3a** exhibit keto-enol tautomerism in both ground and excited states. Compounds **1a-3a** and **1-3** show red shifted absorption as compared to that of **4a** and **4**, devoid of TAB moiety indicating that an effective participation of empty *p*-orbital on boron center in **1a-3a** and **1-3**. Compounds **1** and **2** showed the fluorescence variations in response to the external stimuli such as mechanical grinding. Compounds **1-3** exhibited the phosphorescence with a long lifetime of 18-46 ms. The observed optical properties of **1a-3a** and **1-3** are rationalized in the context of quantum mechanical calculations.

Introduction

Luminescent materials have received a lot of attention owing to their potential applications in OLEDs,^[1] lasers,^[2] sensors,^[3] smart materials,^[3,4] and imaging.^[5] The electronic and optical properties of all carbon materials can be fine-tuned by incorporating main group elements (B, N, O, P, Si, S etc) in their molecular structure.^[6] Among them, research on boron containing luminescent compounds have received considerable interest because of their excellent properties and promising applications in both material science and biology.^[5,7-9] Boron can form three coordinate (borane) and four coordinate (borates) compounds. Triaryl borane (TAB) containing small molecules find applications in linear and non-linear optics,^[10] anion sensing,^[11,12] organic optoelectronic materials,^[13,14] imaging agents,^[15] and optical thermometer.^[16] Recently, studies on photochemistry of tricoordinate boron (TCB) revealed new insights into the light induced molecular rearrangements.^[17,18] Synergetic effects of metal to ligand charge transfer (MLCT) and $\pi(\text{aryl})-\text{p}(\text{B})$ CT interactions in TAB appended metal complex systems have been explored for developing strongly luminescent molecular systems.^[19,20] Considerable research efforts have been devoted to understand the electronic effect of change in geometry of boron center (planar to pyramidal) in rigid and constrained π -conjugated systems having boron atom(s).^[21-25] In this context we have also explored TAB moieties for developing room temperature phosphorescence (RTP) molecular systems,^[26] sensing and imaging of thiophenols in the intracellular environment.^[27]

On the other hand, large amount of research on four coordinate boron compounds is largely driven by their intriguing optical properties and potential applications. For instance, BODIPYs (boron dipyrromethenes) are versatile dyes bearing four-coordinated boron moiety and offer excellent opportunities in various functional applications.^[28-32] But the main challenge with the BODIPY dyes are the tedious synthesis, low reaction yields and weak luminescence in solid-state due to very tight packing combined with a small Stokes shift that leads to self-quenching through energy transfer.^[33,34] To overcome these limitations of BODIPYs and to meet the demand for new emissive materials, new families of tetracoordinated boron compounds with N-B-C,^[35-39] N-B-O^[28,40-45] and O-B-O^[46-48] connectivity has been investigated. Recently, fascinating optical features such as dual,^[31] tricolor,^[32] white-light emission,^[49] self-calibrating ratiometric anion sensing^[50] were realized with TAB appended BODIPY compounds.

Conversely, Schiff bases, a simple class of molecules are obtained by condensation of an amine and a carbonyl compound. When they are synthesized from anilines/ substituted anilines and aromatic carbonyls, they are often called anils. An interesting photochemical process such as an excited state intramolecular proton transfer (ESIPT) and keto-enol tautomerize are often attached with anils.^[51] Anils based ESIPT active molecules have been exploited for developing white light emitters, fluorescence imaging agents, proton transfer lasers and organic light-emitting diodes (OLEDs).^[52-54] Anils can easily be converted to -BF₂ complexes (boranils). Unlike anils, boranils are underexplored, however, intriguing optical properties and proposed application in various field makes boranils an interesting candidate to investigate in detail. For example, diphenylamine appended boranil derivative was developed with unique aggregation induced emission characteristics and exploited in specific imaging of lipid droplets in living cells.^[43] Liu and coworkers demonstrated the antioxidation and tribological properties of boranil based lubricant additives.^[55] In 2013, Raymond Ziessel and coworkers developed a red emissive substituted boranil.^[28]

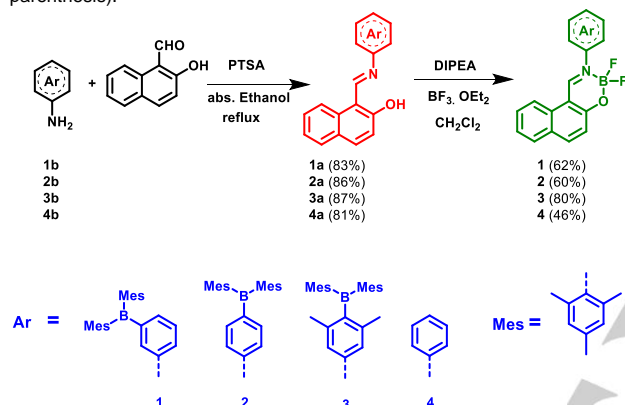
Considering interesting optical properties and applications of boranils together with our recent success with TAB-BODIPY conjugates (intriguing multiple emission feature and sensing characteristics) encouraged us to investigate the effect of incorporation of electron deficient TAB on optical properties of anils and boranils. Accordingly, we designed and synthesized a series of TAB appended anils (**1a-3a**) and their corresponding boranils (**1-3**). The electronic interaction between TAB and anils/boranils in **1a-3a** and **1-3** were finetuned by changing the position of the boryl moiety on the phenyl spacer connecting TAB and anils/boranils units. The effects of steric crowding on the optical and electroinc properties of the newly synthesised conjugates were also studied. The comprehensive outcome of these studies were reported in this manuscript.

Results and Discussion

Synthesis and Characterization:

Compounds **1b-3b** were synthesized by following the reported literature procedures elsewhere.^[56,57] TAB coupled anils **1a-3a** were synthesized by using modified literature procedure,^[51] which involves condensation of β -hydroxynaphthaldehyde with corresponding borylanilines (**1b** for **1a**, **2b** for **2a** and **3b** for **3a**) in ethanol under refluxing conditions (Scheme 1). The model compound **4a**, anil without a TAB moiety was synthesized by following the procedure reported by Ohshima *et al.*^[51] TAB coupled boranils **1-3** and **4** were synthesized by allowing to react $\text{BF}_3 \cdot \text{OEt}_2$ and corresponding anil (**1a** for **1**, **2a** for **2**, **3a** for **3** and **4a** for **4**) in the presence of diisopropylethylamine as base at 0°C (Scheme 1). Analytically pure compounds were obtained in moderate yields after column chromatography followed by recrystallization.

Scheme 1. Synthesis of **1a-4a** and **1-4** (reaction yields are shown in parenthesis).



The structural and optical features of **4a** were studied in detail by Ohshima and coworkers.^[51] However, the corresponding boranil compound **4** was not reported elsewhere. Thus, for comparative studies both **4a** and **4** were synthesized and fully characterized. All compounds were characterized by NMR spectroscopy (^1H , ^{13}C , ^{11}B and ^{19}F) and high-resolution mass spectrometry (HRMS). The formation of **1a-4a** were confirmed by the presences of ^1H resonances around ~ 15.5 ppm corresponding to the enolic $-\text{OH}$ group and signature resonance of imine proton $-\text{CH}=\text{N}$ at -9.22 ppm. ^1H resonances of *ortho*- and *para*- CH_3 groups of mesityl moieties attached to boron at -2.04 - 2.33 ppm further confirms the formation of TAB appended anils. In ^{11}B NMR spectra, **1a**, **2a** and **3a** showed resonances at 74.4, 73.4, 74.2 ppm respectively corresponding to the tricoordinate boron; and the values are comparable to the ^{11}B resonances for other triarylboron and borylanilines reported elsewhere.^[56-58] In boranil complexes **1-4**, the imine proton resonances are shifted upfield as compared to that of the corresponding anils. The signal corresponding to enolic OH disappeared in **1-4**, further, these compounds show two ^{11}B signal corresponding to tri (singlet) and tetra (a triplet) coordinate boron centers unequivocally confirms the formations of TAB appended boranils. The intensity of ^{11}B signals of tricoordinate boron is significantly lower as compared with the ^{11}B resonance of tetracoordinate boron in these compounds. ^{19}F signals corresponding to $-\text{BF}_2$ moiety of **1-4** observed at ~ -134 ppm. Interestingly, **3** with meta-xylene spacer showed two distinct set of resonances for fluorine of $-\text{BF}_2$ unit which clearly indicates that the two fluorine atoms are magnetically nonequivalent. Methyl groups in the phenyl spacer connecting $-\text{BMes}_2$ moiety and Schiff-base fragment in **3** imposed additional structural constrain, consequently the molecular free rotation arrested and the two fluorine atoms become magnetically non-equivalent.^[59]

Molecular structures

Single crystals of **1a-3a** and **1-3** suitable for single crystal x-ray diffraction studies were obtained by slow evaporation of corresponding solutions under ambient conditions (**1a** from acetone, **2a** and **3a** from mixture of chloroform/methanol (1:4), **1** and **2** from mixture of dichloromethane/methanol (1:4) and **3** from chloroform/ethanol (1:4)). Molecular structure of **1a-3a** and **1-3** are shown in Figure 1. Crystallographic diffraction data, important bond lengths, bond angles and torsion angles are depicted in ESI (Table S1-S7). Compounds **1a**, **2a**, **1** and **3** were crystallized in triclinic crystal system with $P-1$ space group, whereas **2** and **3a** are crystallized in monoclinic crystal lattice with $P2_1/c$ and Pn space group, respectively. Compound **1a** is crystallized in enolic form (E-OH) with strong H-bonding interaction between enolic $-\text{OH}$ and imine N ($\text{H} \cdots \text{N}$ distance = 1.698 Å). The C2-O1 and C11-N1 bond distances are 1.341 and 1.293 Å respectively. Whereas, for **2a** and **3a** their keto forms (Z-NH) dominated in the crystal lattice. The C2-O1 bonds (1.285 Å for **2a**, 1.282 Å for **3a**) are shortened and C11-N1 bonds (1.306 Å for **2a**, 1.317 Å for **3a**) are elongated as compared to that of **1a**. These bonding parameters are comparable with the values reported for **4a** and other substituted Schiff bases (Figure S42 Table S3, S5 and S7).^[60] The H-bonding interactions are weaker for **2a** (1.817 Å) and **3a** (1.782 Å) as compared to **1a** (1.698 Å).

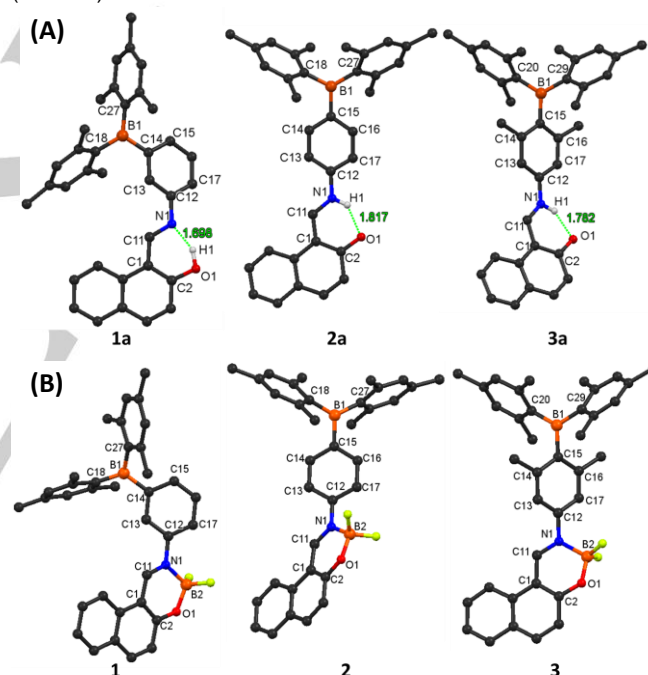


Figure 1. Molecular structures of (A) **1a-3a** and (B) **1-3** with atom numbering scheme. Except phenolic/amine hydrogen, all the other hydrogen atoms are removed for clarity.

The sum of the three C-B-C angles around the boron atom of TAB in **1a-3a** and **1-3** are $\sim 360^\circ$ indicating trigonal planar configuration similar to that of borylanilines (**2b** and **3b**)^[57] and other TAB based D-A systems reported elsewhere.^[58,61] The B1-C15 bond in **3a** (1.578 Å) and **3** (1.593 Å) are elongated as compared to that in **1a** (1.567 Å), **2a** (1.567 Å), **1** (1.583 Å) and **2** (1.565 Å), owing to the steric congestion imposed by the meta-mesityl spacer in **3a** and **3**. Further, the B1-C15 bonds in **1a-3a** are elongated compared to that of borylanilines **2b** (1.538 Å) and **3b** (1.578 Å).^[57] The N1-C12 bond lengths in **1a**, **2a** and **3a** are 1.414 Å, 1.406 Å and 1.415 Å, respectively which are shorter than the bond lengths in **1** (1.442 Å), **2** (1.434 Å) and **3** (1.430 Å). These results clearly indicate that both Schiff base formation and $-\text{BF}_2$ coordination weakens the electronic communication

between the boryl group and aryl amine moiety. The dihedral angle between -BC2 (Mes₂) plane and of the phenyl spacer are 25.38° (**1a**), 22.96° (**2a**), 50.62° (**3a**), 36.20° (**1**), 32.98° (**2**) and 54.24° (**3**). Based on these results, it can be tentatively concluded that the donor-acceptor interactions are stronger in **2a** and **2** as compared to other compounds but are weaker than that observed in corresponding borylanilines.^[57]

UV-Vis absorption Studies

Compounds **1a-3a** show two major absorption bands in the region 280-400 nm and weak absorption band at ~450 nm in cyclohexane solutions (Figure 2). Absorption bands in **2a** and **3a** are red shifted than that in **1a**. This can be attributed to the better electronic conjugation through the empty p_π orbital of boron center in para position of phenyl spacer in **2a** and **3a** as compared to that of **1a** with the boryl unit connected at the meta position of the phenyl spacer. In contrast to **1a-4a**, compounds **1-4** show only two absorption bands in cyclohexane solutions. Upon -BF₂ complex formation, the weak band at ~450 nm in **1a-4a** disappeared in **1-4**. The absorption bands in **1-4** are red shifted compared to their respective anils **1a-4a**. The absorption spectral features of TAB coupled anils (**1a-3a**) and boranils (**1-3**) are like that of model compound **4a** and **4** which are devoid of boryl moiety. However, the absorption bands in **1a-3a** and **1-3** are significantly red shifted and showed enhanced molar absorptivity as compared to **4a** and **4** respectively (Table S8 and S9). This result indicating the involvement of empty p-orbital in TAB in extending the conjugations in **1a-3a** and **1-3**.

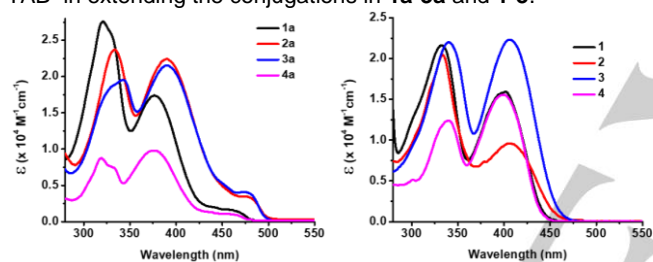


Figure 2. UV-Vis absorption spectra of **1a-4a** (left) and **1-4** (right) in cyclohexane (concentration = 10 μM).

To get an insight into the origin of multiple UV-Vis absorption bands in these compounds, absorption spectra of **1a-4a** and **1-4** were studied in solvents of different dielectric constants (Figure S43). For **1a-4a**, increase in solvent polarity decrease the intensity of the band at ~380 nm, concomitantly the intensity of the band at the red end of the spectrum increases. Further, in polar protic solvent such as methanol the band at ~380 nm completely vanished. Based on these studies and literature reports it can be concluded that keto-enol tautomerization takes place in the ground state of **1a-4a** and the compounds exist as a mixture of trans-enol form (E-OH form) and cis-keto form (Z-NH form) in solutions (Scheme S1).^[51] Thus, the absorption bands around 450 and 470 can be attributed to the Z-NH form and the bands around 380 arises from the E-OH form.^[51] The absorption events of **1-4** did not show significant changes in spectral features in solvents of different polarity. Calculated HOMO-LUMO energy gap for **1a-4a** and **1-4** follow the trends **4a>1a>3a>2a** and **4>1>3>2** as observed in UV-vis absorption studies. Based on the experimental and TD-DFT results, the absorption band around ~320 nm in **1a-4a** can be assigned to combination of π-π* and π-p(B) transitions. Whereas that around ~380 nm can be attributed to the n(N)-π* transition combined with N-B charge transfer transition.

Computational

To get more insight into the electronic structures and optical properties, DFT calculations were performed with B3LYP hybrid

Studies

functional and 6-31G(d) basis set for all the atoms as incorporated in Gaussian 09 software.^[62-66] Both keto and enol forms of **1a-4a** and **1-4** were optimized to their minimum potential energy surface in ground state (Figure 3, S53). The metric parameters of DFT optimized structures are comparable with the respective molecular structures obtained from single crystal X-ray diffraction studies. The energy difference between the ground state optimized structures of the enol and the keto-form is very less (0.04 eV for **1a**, 0.03 eV for **2a**, 0.04 eV for **3a** and 0.02 eV for **4a**); since, the energy difference between both the forms is small consequently both the forms present in the ground state as inferred from UV-Vis absorption studies (Table S16).

Both enol (E-OH) and Z-NH (keto) form of **1a-4a** showed similar frontier molecular orbital (FMO) distributions (Figure 3 and S53). Highest occupied molecular orbitals (HOMOs) of **1a-3a** are mainly delocalized over the phenylimino-naphthol moiety. While the lowest unoccupied molecular orbitals (LUMOs) are delocalized over the phenylimino-naphthol moiety with a significantly large contribution from the boron of TAB moiety. While the FMOs of **4a** delocalized over the entire molecule, clearly indicates that UV-Vis absorption features originate from π-π* state and n-π* states in **4a**. In the ground state optimized structures of keto forms (Z-NH) of **1a-4a**, the naphthalene ring and the phenyl spacer adopt coplanar arrangements (except the -BMe₂ moiety). As a result of the extended conjugation, the HOMO-LUMO gap in Z-NH form decreased as compared to E-OH form and thus red-shifted absorption bands observed for the Z-NH form.

For compound **1**, FMOs are distributed over the naphthalene ring, oxazaborinine ring and phenyl spacer, however, no contribution from the -BMe₂ unit (Figure 3). Whereas for **2** and **3** HOMOs are delocalized over the whole molecules except the boron atom of -BMe₂ unit, while LUMOs are delocalized over the naphthalene ring, oxazaborinine ring and phenyl ring with significant contribution from the empty p_π-orbital of the boron atom of TAB. The FMOs of **4** delocalized over the entire molecule as like in **4a**. The HOMO-LUMO gap follows the trend **4>1>3>2** for alike the TAB coupled anils; this results in line with the trend observed in UV-Vis absorption spectra of these compounds. Compared to **1a** and **4a**, compounds **1** and **4** showed decreased HOMO-LUMO gap owing to the stabilization of both HOMOs and LUMOs, this results directly corroborate the red shifted UV-Vis absorptions for **1** and **4** as compared to that of **1a** and **4a**. Similar red shifted absorption features were observed for **2** and **3** as compared to **2a** and **3a**, although their HOMO-LUMO gaps do not comply with this observation.

Photoluminescence Studies

Photoluminescence (PL) features of **1a-4a** and **1-4** are studied in cyclohexane solutions (conc.= 10 μM, Figure 4). Compound **4a** is very weakly emissive (λ_{em} = 360 nm) as reported by Ohshima *et al.*^[51] Upon excitation at 310 nm, **1a**, **2a** and **3a** show emission band at 403, 363 and 375 nm, respectively. In addition to the major band, **2a** and **3a** showed a weak band in the lower energy region around 490 nm. Compounds **1**, **2**, **3** and **4** show broad emission band at ~450, ~403, ~459 and ~480 nm respectively (λ_{ex} = 340 nm). TAB coupled boranils showed red shifted emission and higher Stokes shift compared to corresponding anils, this can be attributed to reduced HOMO-LUMO energy gap in the former. Photoluminescence quantum yield (PLQ) of these compounds are found to be 0.21, 0.26, 0.70, 2.62, 13.75, 2.50 and 0.76% for **1a**, **2a**, **3a**, **1**, **2**, **3** and **4** respectively. PLQ of TAB coupled boranils are higher as compared to that of corresponding anils, may be due to the structural rigidification after -BF₂ complexation, which minimizes the non-radiative decay channels caused by structural isomerization and geometrical relaxations.

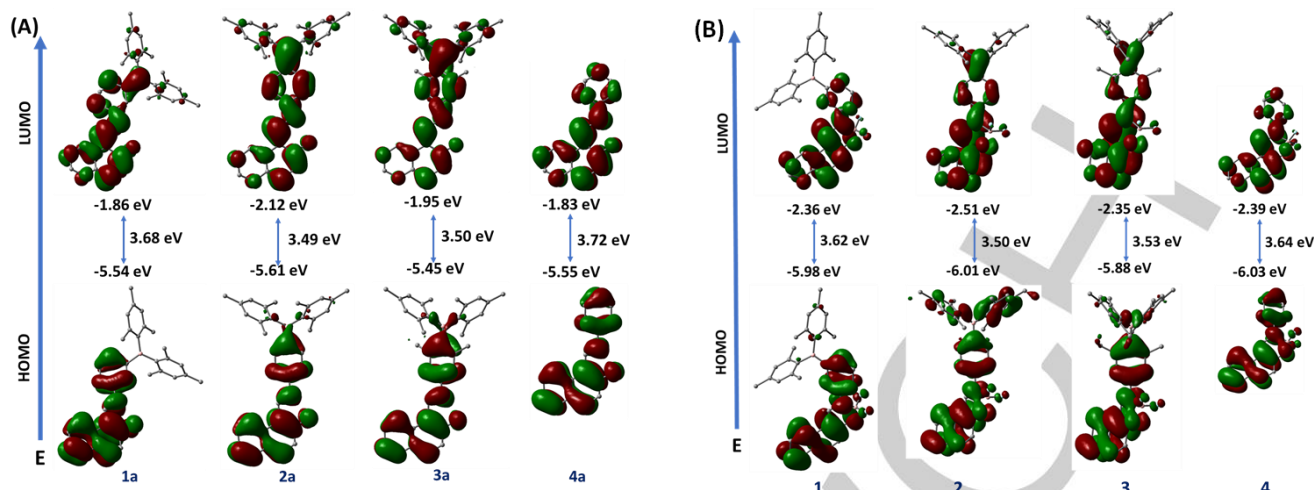


Figure 3. Frontier molecular orbitals and the orbital energies (eV) for (A) **1a-4a** (E-OH) and (B) **1-4**. Energy levels are not to the scale. Atom color codes: C (grey), B (orange), N (blue), O (red). Hydrogen atoms are omitted for clarity.

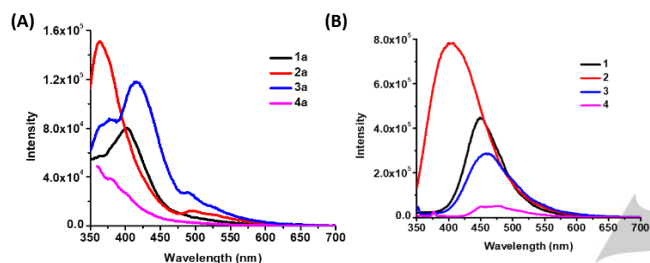


Figure 4. Fluorescence spectra of **1a-4a** (A) ($\lambda_{\text{ex}} = 310$ nm, conc. 10 μM) and **1-4** (B) ($\lambda_{\text{ex}} = 340$ nm, conc. 10 μM) in cyclohexane.

To get better insight into the nature of emissive state of these compounds, PL measurements have been carried in solvents of varying polarity (Figure S44, Table S8 and S9). For **1a-3a**, upon increasing the solvent polarity, bathochromic shift in emission maxima was observed. Furthermore, **1a-3a** exhibit dual emissions. To understand the dual emissive nature of **1a-3a**, their emission spectra were recorded in nonpolar cyclohexane and polar protic methanol solvent at various excitation wavelengths (Figure S45). When the cyclohexane solutions were excited at ~ 310 nm, strong emission band at ~ 400 nm and weak band at ~ 500 nm were observed. Whereas, upon excitation at ~ 450 nm, only the weaker emission band at ~ 500 nm was observed. Methanol solutions show weak band around 400 nm and intense band at around 500 nm independent of the excitation wavelength. Based on this results, one can tentatively assign that the emission bands at ~ 400 and ~ 500 nm originate from the E-OH and Z-NH forms of the compounds, respectively. Similar to ground state, the E-OH form dominates in cyclohexane and Z-NH form dominates in methanol in the excited state. The higher Stokes shift in this kind of Schiff base compounds are usually explained by an excited state intramolecular proton transfer (ESIPT) process.^[53,67-70] The possibility of ESIPT in **1a-3a** can be confirmed by the absence of 500 nm emission band in cyclohexane and 400 nm band in methanol. The positive emission solvatochromism of **1a-3a** with increasing solvent polarity clearly indicates that the excited state of both trans-enol (E-OH) and cis-keto form (Z-NH form) have charge transfer characteristics. Further, excited state lifetime measurements were carried out on **1a-3a** in non-polar cyclohexane, polar dichloromethane and polar protic methanol solvent, the results also confirmed the CT characteristics of the excited states. For all the molecules, there were multiple emissive species in the excited state are observed, indicating

the presence of both keto and enol isomers in solutions. For **1a**, The average lifetime measured at the emission maxima in cyclohexane, dichloromethane and methanol are 7.05, 21.82 and 14.35 ns, respectively. The decrease in lifetime in methanol may be due to the increase in non-radiative decay pathways triggered by H-bonding interactions between **1a** with methanol. Similar observations were noted for **2a** and **3a**.

For **1-3**, a bathochromic shift in emission maxima with a weakening of luminescence intensity was observed upon increasing the solvent polarity, points to the charge transfer nature of the emissive state. The extent of solvatochromic shift is maximum for **2** and minimum for **1**. Furthermore, excited state lifetime measurements in cyclohexane, dichloromethane and methanol revealed the presence of multiple emissive species in the excited states of **1-3** (Table S8 and S9). The average lifetimes recorded for **1** is 15.94, 17.77 and 7.65 ns in cyclohexane, dichloromethane and methanol, respectively. These studies further confirm the involvement of CT excited state in the emission process.^[71] Similar results were observed for **2** and **3** as well. Model compound **4** showed blue-shifted weaker emission as compared to the TAB coupled boronils **1-3**. Average lifetime recorded for **4** is 1.31, 1.19 and 0.85 ns in cyclohexane, dichloromethane and methanol, respectively. Compound **4** did not show any solvatochromic luminescence characteristics. These results indicated that the presence of boryl moiety in **1-3** facilitate the formation of lower energy CT state in these compounds as compared with **4** devoid of boryl moiety.

Solid state emission and stimuli responsive luminescence characteristics

All the compounds showed vivid emission in the solid state (Figure 5, S47). Most often planar organic π -systems are brightly emissive in solutions, however, their emission intensity is weakened or fully quenched in the solid state because of face-to-face strong π - π interactions, which facilitates the nonradiative decay.^[72,73] In case of **1a-3a** and **1-3** the presence of sterically demanding bimesityl group expected to stop the unwanted strong face-to-face π - π interactions in the solid state. As expected no face-to-face π - π interactions were observed in crystal structures of **1a-3a** and **1-3** however, because of the presence of large naphthyl π -system slipped π - π and C-H \cdots π interactions were observed in the crystal structures of **1a-3a** and **1-4** (Figure 6 and S36-S41). Upon excitation at 400 nm, **1a** shows a narrow yellow emission band with emission maxima at 530 nm. Compounds **2a** and **3a** show much red shifted and broader emission band with emission maxima at ~ 675 and ~ 640

nm respectively. Compound **4a** shows narrow yellow emission band peaked at ~538 nm very similar to **1a**. The significant bathochromic shift and broadness in emission spectra of **2a** and **3a** as compared to **1a** can be explained with the help of careful analysis of their crystal structures. The dihedral angle between the phenyl ring and the naphthyl ring is less for **2a** (9.08°) and **3a** (23.59°, 11.76°) as that of **1a** (31.32°) (Table S4) (in **2a** and **3a** naphthyl and phenyl units adopt coplanar arrangements). As a result stronger intermolecular hydrogen bonding and $\pi\cdots\pi$ interactions were observed in **2a** and **3a** as compared to **1a** with twisted structure (Figure 6A, B and C). Thus, the strong intermolecular slipped $\pi\cdots\pi$ interactions should be responsible for the observed bathochromic shift and broadness in emission spectra of **2a** and **3a**. Further, the planar arrangements of chromophores in **2a** and **3a** can facilitate the strong conjugation through vacant *p*-orbital of B of TAB moiety in para position of the phenyl spacer better than in **1a** with boron moiety in *meta*-position of the spacer.

Boranils **1-4** show blue shifted emission as compared to their corresponding anils **1a-3a**. The BF_2 complexation rigidifies the structure and inhibit the molecular motions consequently PL of **1-3** shifted blue (Figure 6). Compound **1** show green color emission with peak maximum at ~496 nm. Whereas **2** showed orange emission (λ_{max} ~535 nm) and **3** has greenish yellow emission at ~514 nm. Boranil **4** exhibit greenish emission at ~504 nm similar to **1**. For both anils **1a-4a** and corresponding boranils **1-4**, the wavelength of maximum emission intensity follows the trend **2a**>**3a**>**4a**>**1a** and **2**>**3**>**4**>**1**. The absolute PL quantum yields of **1a**, **2a**, **3a**, **4a**, **1**, **2**, **3** and **4** are found to be 1.80, 0.93, 0.56, 4.64, 6.63, 1.63, 5.95 and 4.06% respectively (Table S10 and S11). Lower PL quantum yield observed in **2a** and **2** indicate that the nonradiative decay is strongly operative in these molecules as compared with other compounds.

Time-correlated single photon counting (TCSPC) measurements on these compounds were performed to determine the excited state lifetime. All the compounds show biexponential decay in the solid state (Table S10, S11 and Figure S48, S49). The average lifetime were obtained as 1.17, 3.40, 3.84, 2.85 ns for **1a**, **2a**, **3a**, **4a** and 2.83, 2.16, 1.66, 2.54 ns for **1**, **2**, **3** and **4** respectively. The non-radiative (k_{nr}) decay rate constants are significantly larger than the radiative (k_{r}) rate constants calculate for these compounds, which indicates that these molecules lose most of their excited state energy through non-radiative relaxation (Table S10 and S11).

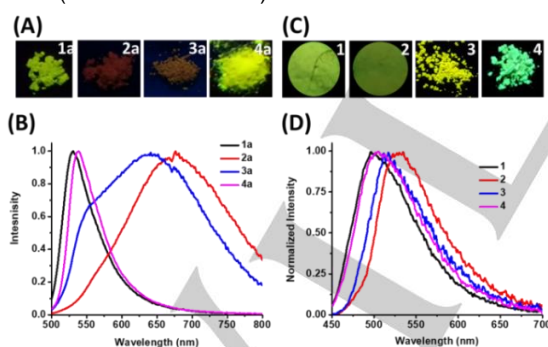


Figure 5. Normalized emission spectra of (B) **1a-4a** and (D) **1-4** ($\lambda_{\text{exc}} = 400$ nm) in solid state. Digital photographs of solids of **1a-4a** (A) and **1-4** (C) under 365 nm UV light illumination.

Pristine solids and single crystals of **1** and **2** showed different emission features. This clearly indicates that the emission features of these compounds are governed by intermolecular interactions. Thus, the emission characteristics of **1-3** under various external stimuli like pressure, solvent vapors and temperature were carried out. Interestingly, **1** and **2** show changes in emission color upon mechanical grinding, whereas **3** did not show significant response to mechanical stimuli. As prepared sample of **1** show green emission with maximum at ~520 nm, whereas the crystals of **1** show red shifted orange

emission with maximum at ~546 nm (Figure 7A, B and C). Upon grinding the crystals, the emission maxima shifted to ~512 nm. When the ground samples were fumed with DCM solvent vapors the emission band broadened and the intensity of the peak at 546 nm increased. Compound **2** also showed similar mechano-responsive luminescence characteristics (Figure 7D, E and F). Pristine solids of **2** exhibit yellow color emission with maximum at ~528 nm with a shoulder band at 495 nm. Crystals of **2** show only 528 nm band. The ground sample of **2** show green emission at ~495 nm. When the ground sample was fumed with DCM, the emission maximum shifted to 504 nm and a hump at ~528 nm is observed. These results indicate that restoration crystallinity upon DCM fumigation is slow consequently complete recovery of PL of crystalline solid was not observed.

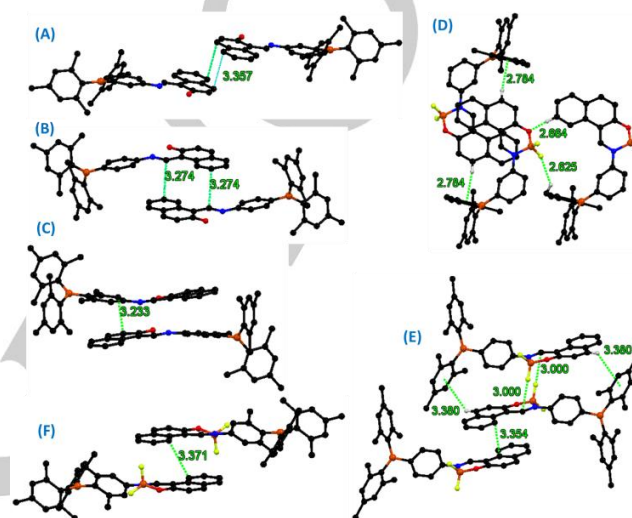


Figure 6. Depiction of an intermolecular interactions (distance in Å) present in the crystal structure of (A) **1a**, (B) **2a**, (C) **3a**, (D) **1**, (E) **2** and (F) **3**. All the H-atoms except the atoms involved in intermolecular interaction are removed for clarity. Colour codes: C - black, N - blue, O - red, B - saffron and F - yellow.

Absolute PLQ and excited state lifetime measurements were carried out on the crystals and ground samples of **1** and **2**. The ground samples of both the compounds show increased PLQ and PL lifetime (Table S12, Figure S50). The calculated radiative and non-radiative decay rate constants also well corroborated with the observed PLQ and excited state lifetime data. To further understand the mechano-responsive luminescence features of these compounds, powder x-ray diffraction patterns were recorded for the crystals, as prepared sample and ground samples of both **1** and **2** (Figure 7). Both pristine and single crystals of **1** and **2** showed intense reflection peaks, indicative of the crystalline nature of these samples. However, the positions of diffraction peaks for both pristine and crystals of these compounds are significantly different pointing to the fact that long range ordering of the molecules in pristine and single crystals are different. Ground samples of these compounds show more diffused peaks indicating the reduced crystallinity as compared to pristine and single crystals. These results indicate that the emission colours of **1** and **2** in solid state is dictated by the intermolecular interactions between the neighbouring molecules. From the crystal structure of **1** and **2** it is clear that these compounds form a supramolecular structures via a series of intermolecular interactions such as C-H \cdots π , $\pi\cdots\pi$, and F $\cdots\pi$ in (Figure 6D, E and S39, 40). In **1** and **2** the boron is connected with boranils via simple phenyl spacer (with out substituent), thus, the mechanical stimuli may alter their crystal packing by altering the intermolecular interactions and consequently alter their luminescence colour. However, in **3** the presence of two methyl groups on the phenyl spacer connecting the boron and boronil moieties may hinder the intermolecular rearrangements in the

solid state and consequently its PL features insensitive to mechanical stimuli.

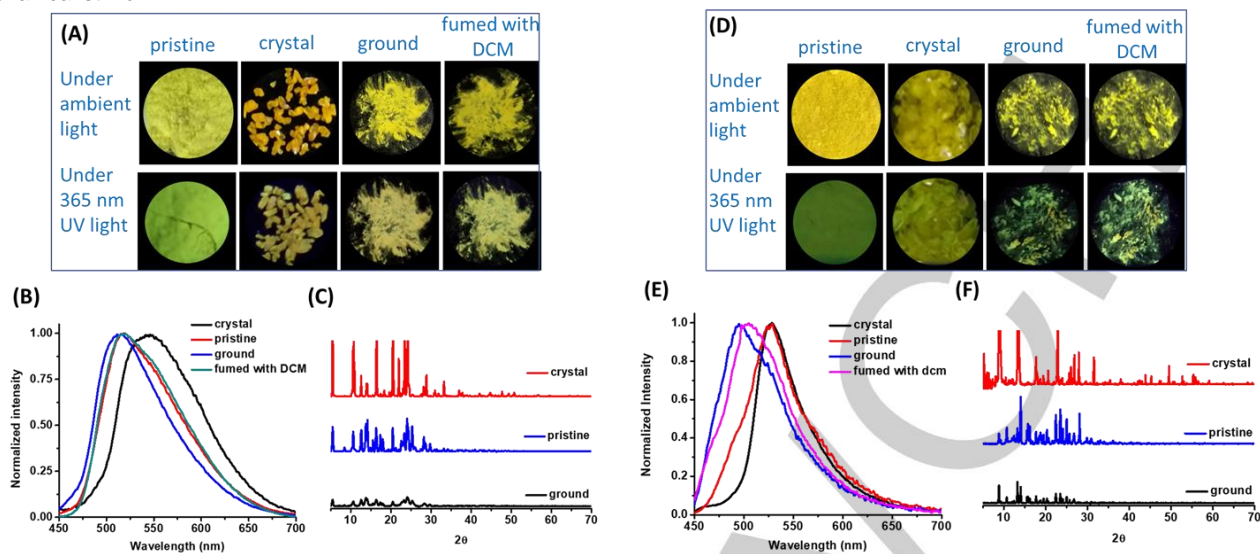


Figure 7. (A) The digital photograph of solids (pristine solids, single crystals, ground solids before and after DCM fumigations) of **1** under 365 nm UV-light illumination. (B) PL spectra of solids (pristine solids, single crystals, ground solids before and after DCM fumigations) of **1**. (C) powder XRD pattern of different samples of **1** ($\lambda_{\text{ex}} = 400$ nm). (D) The digital photograph of solids (pristine solids, single crystals, ground solids before and after DCM fumigations) of **2** under 365 nm UV-light illumination. (E) PL spectra of solids (pristine solids, single crystals, ground solids before and after DCM fumigations) of **2**. (F) powder XRD pattern of different samples of **2** ($\lambda_{\text{ex}} = 400$ nm).

Phosphorescence

The PL spectra of solids of **1**, **2**, **3** and **4** shifted red significantly as compared to their respective PL spectra in solutions pointing to the fact that the intermolecular interaction indeed plays a role in controlling the PL feature of these compounds. To comprehend the PL feature of these compounds both steady state and time-resolved PL decay kinetics studies on these compounds were performed at 77 K and the results were compared with the PL features at room temperature. Compounds **1**, **2**, **3** and **4** showed strong PL at 77 K as compared to PL obtained at 298 K. The lower PL quantum yield of these compounds clearly indicated that non-radiative decay of the excited state is strongly operative in these compounds. One of the most common non-radiative decay channels is the triplet-mediated excited state deactivation process. To get insight into the role of triplet states in the PL feature of these compounds, prompt and delayed spectra were recorded both at 298 and 77 K. All the compounds showed very weak delayed spectra at 278, however, strong and dual emission (496 and 600 nm for **1**, 535 and 620 nm for **2**, 514 and 635 nm for **3** and 504 and 610 nm for **4**) was observed for all the compounds at 77 K. The prompt and delayed spectra of all the compounds obtained at both 298 and 77 K (lower wavelength band) overlapped smoothly. The temperature-dependent delayed emissive characteristics (weak PL at 298 K and strong PL at 77 K) of these compounds at low temperature is indicative of involvement of the triplet state in the PL process. PL lifetime of the higher energy phosphorescence band in these compounds were found to be 1.51, 1.23, 1.10 and 1.55 ms respectively for **1**, **2**, **3** and **4**. PL lifetime of the lower energy phosphorescence band in these compounds were found to be 46.48, 18.41 and 37.29 ms respectively for **1**, **2** and **4** (lifetime could not be recorded for the lower energy phosphorescence band in **3** due to very low counts). Temperature-dependent both steady state and time-resolved PL studies confirmed the involvement of the triplet state in the emissive process. Further, the selective appearance of a delayed PL band in the red end of the phosphorescence spectra of these compounds is attributed to the emission from the triplet state of intermolecular origin.

Phosphorescence features of TAB compounds at 77 K have been previously reported independently by Marder,^[74] Wang,^[75,76] and Yamaguchi.^[77] Fraser and coworkers reported the room temperature phosphorescence (RTP) of boron diketonate complexes in a polymer matrix.^[78] To the best of our knowledge, this result is the first report on the phosphorescence of TAB-coupled boranils.

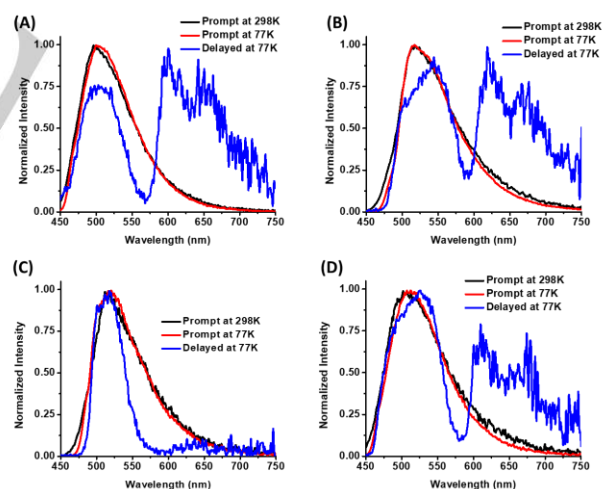


Figure 8. Prompt (at 298 K and 77 K) and delayed emission (at 77 K) spectra of thin films of (A) **1**, (B) **2**, (C) **3** and (D) **4** ($\lambda_{\text{ex}} = 400$ nm).

Achieving phosphorescence from a purely organic molecule is not common as most of them have a singlet ground state and the phosphorescence process requires efficient intersystem crossing (spin-forbidden) from singlet to triplet ($S_n \rightarrow T_n$) in the excited state with reduced non-radiative decay ($T_n \rightarrow S_0$). TD-DFT calculations were performed with the coordinates obtained from the single crystal X-ray structure to get the energies of singlet and triplet vertical transitions and to find out the possible intersystem crossing channels (ISC). The main ISC channels of a molecule are supposed to follow the conditions like i) the orbital configuration of energy between the first excited singlet (S_1) and any of the triplet

excited states (Tn) should be same and the ratio of electronic transition should be higher among various possible transition orbital compositions. And ii) the difference in energy between the S1 and Tn should be in the range of 0.1-0.4 eV. The calculated energy levels in **1-3** are illustrated in Figure S54. The major ISC channels are S₁ → T₆ for **1**, S₁ → T₃ for **2** and S₁ → T₂ for **3**.

Conclusion

A new class of TAB coupled anils **1a-3a** and their corresponding boranil complexes **1-3** are synthesized and structurally characterized. Incorporation of Lewis acid TAB into anils (**1a-3a**) and boranils (**1-3**) increase the π-conjugation through empty p orbital on tricoordinate boron and consequently shift the UV-Vis absorption and emission bands to red region as compared to compounds devoid of a TAB moiety (**4a** and **4**). TAB coupled anils (**1a-3a**) showed solvent polarity dependent UV-Vis absorption and emission characteristics corresponding to their enol (E-OH) and keto (Z-NH) forms. All the compounds showed vivid emission colors in the solid state and interestingly **1** and **2** showed mechanoresponsive luminescence features. Compounds **1-4** showed phosphorescence in the solid-state with longer lifetime (18-46 ms). These studies reveal that one can fine-tune the optical properties of anils and boranils by systematically changing the nature of the spacer between these molecular partners (TAB and anil/boranil) and the position of the TAB unit on the spacer moiety (meta and para). Structure property correlations drawn from this study will pave the way for the designing better luminophores.

Experimental Section

Materials and methods

Chemicals were purchased from commercial sources (Spectrochem, India; SDFCL, India; Merck, Germany; Aldrich, USA) and used without further purification, unless otherwise stated. DCM was dried over CaH₂ and stored over 4Å molecular sieves prior to use. Diisopropylethylamine (DIPEA) was dried over KOH and sodium followed by distillation under argon atmosphere and stored over 4Å molecular sieves. Reactions were carried out using Standard Schlenk-line technique.

¹H and ¹³C NMR spectra were recorded at 25 °C on a Bruker Avance 500 MHz NMR Spectrometer operating at a frequency of 500 MHz for ¹H and 126 MHz for ¹³C. ¹H NMR spectra were referenced to TMS (0.00 ppm) as an internal standard. Chemical shift multiplicities are reported as singlet (s), doublet (d), triplet (t), quartet (q), quartet of doublet (dq) and multiplet (m). ¹³C resonances were referenced to the CDCl₃ signal at -77.16 ppm. ¹¹B NMR spectra were recorded at 25 °C on a Bruker Avance 400 MHz NMR Spectrometer operating at a frequency of 128.4 MHz for ¹¹B. ¹¹B NMR chemical shift values were referenced to the external standard boron signal of BF₃·Et₂O. ¹⁹F NMR spectra were recorded at 25 °C on a Bruker Avance 500 MHz NMR Spectrometer operating at a frequency of 470.6 MHz for ¹⁹F. ¹⁹F NMR chemical shift values were referenced to the external standard fluorine signal of CFCl₃. High resolution mass spectra (HRMS) were recorded on an Agilent Q-TOF LCMS by electrospray ionization (ESI) method.

Sample preparation for spectral measurements were carried out using microbalance (± 0.1 mg precision), spectrophotometric grade solvents and standard volumetric glasswares. Quartz cuvette was used for the study of optical properties in solution state and was sealed with screw cap during measurements. A SHIMADAZU UV-2600 spectrophotometer was used to record UV-Vis absorption spectra. An Edinburgh Instruments FLS980 spectrometer was used to record emission and excitation spectra. The spectrometer was equipped with a double monochromator for both excitation and emission operating in right-angle geometry mode and the highly sensitive photomultiplier tube (RED PMT in Cooled

Housing) was positioned after a double emission monochromator. All the spectra were corrected considering the spectral response of the instrument. The same FLS980 spectrometer connected to an Oxford Instruments Mercury iTC temperature controller and equipped with an Oxford Instruments OPTISTAT DN2 cryostat was used to perform temperature dependent (77 K and 298 K) measurements. Variable temperature measurements were performed only after the equilibration of the samples at each temperature. Time gated emission measurements were carried out using a pulsed microsecond flash lamp (μF1) with a pulse width of 1.1 μs. The delay time scale was 100 μs where in the shorter species having excited state lifetime of ~10 μs will be discarded by the time gated circuit attached to PMT detector. Fluorescence lifetimes were recorded using the time correlated single photon counting (TCSPC) method using the same Edinburgh Instruments FLS980 spectrometer described above. Measurements were made in right-angle geometry mode, and the emission was collected through a polarizer set to the magic angle. Samples were excited with a 375 nm pulsed LED. Phosphorescent lifetimes were measured using the microsecond flash lamp described above. The quality of fitting for all decay curves were examined to be good enough based on the calculated values of the reduced χ² and Durbin Watson parameters and visual inspection of the weighted residuals. Absolute solid-state quantum yields were measured using calibrated Horiba JOBIN YVON Integrating sphere. Solution state quantum yields were calculated with reference to anthracene (φ = 0.27 in EtOH at 27 °C) as standard.^[80]

Single crystal X-ray diffraction (SCXRD) studies were carried out with a Bruker SMART APEX diffractometer equipped with 4-axis goniometer (MoKα, λ = 0.71073 Å) with the help of APEX2 software.^[81] The data integration and reduction were carried out using SAINT,^[82] and an empirical absorption correction was applied with SADABS.^[83] The structures were solved by direct methods and refined by full matrix least-squares on F² using SHELXTL software^[84] and WinGX v2014.1.^[85] SQUEEZE/PLATON program was used to remove the solvents (/disordered solvent) for **2a** (chloroform), **3a** (methanol) and **3** (chloroform) but taking the corresponding scattering contribution into account.^[86] For **3** overall data quality was not good because of poor crystal quality having disordered chloroform molecule in unit cell.

Density functional theory (DFT/TD-DFT) calculations were done using B3LYP functional with 6-31G(d) basis set as incorporated in Gaussian 09 package for all the atoms, mixing the exact Hartree-Fock-type exchange with Becke's exchange functional and that proposed by Lee-Yang-Parr for the correlation contribution.^[62-65] The molecular structures obtained from SC-XRD measurements were taken as the input for the calculations. All ground state geometry optimisations were followed by subsequent frequency test to ascertain stationary points. TD-DFT calculations were performed on the ground state optimized structures to find the singlet and triplet vertical transition energies. The optimized structures and the frontier molecular orbitals (FMOs) were viewed using Gaussview 5.0.8.^[66]

Synthesis

Synthesis of 1a: To a solution of borylaniline **1b** (700 mg, 2.05 mmol) in absolute ethanol (10 ml), catalytic amount of p-toluenesulfonic acid (PTSA) was added. 2-hydroxy-1-naphthaldehyde (360 mg, 2.05 mmol) was dissolved in 10 ml of absolute ethanol and then added to the above amine solution under stirring condition. The resulting mixture was then refluxed for 6 h and the reaction was monitored by TLC. After complete consumption of the reactants; the reaction mixture was cooled to room temperature. The resultant precipitate was isolated by filtration and washed several times with ethanol to get the analytically pure compound (**1a**) as a yellow color solid (Yield = 83%, 845 mg). ¹H NMR (500 MHz, CDCl₃, 25 °C): δ (ppm) 15.45 (s, 1H), 9.22 (s, 1H), 8.01 (d, J = 8.3 Hz, 1H), 7.77 (d, J = 9.05 Hz, 1H), 7.69 (d, J = 7.90, 1H), 7.43-7.52 (m, 5H), 7.32 (t, J = 7.25 Hz, 1H), 7.04 (d, J = 8.85 Hz, 1H), 6.84 (s, 4H), 2.32 (s, 6H), 2.04 (s, 12H). ¹³C NMR (126 MHz, CDCl₃, 25 °C): δ (ppm) 171.6, 154.3, 144.7, 141.6, 141.0, 1392, 137.1, 134.3, 133.4, 129.5, 129.5, 128.5, 128.2, 127.7, 127.4, 123.6, 123.0, 122.8, 118.9, 108.8, 23.6, 21.4. ¹¹B NMR (128 MHz, CDCl₃, 25 °C): δ (ppm) 74.4. ESI-MS, (positive ion mode): calcd for C₃₅H₃₄BNO 495.2733 Da, observed 496.2811 [M+H]⁺.

Synthesis of 2a: Compound **2a** was synthesized following the same procedure as described for **1a**. Quantities of the reactants/reagents used and the characterization data as follows: Borylaniline **2b** (1.54 g, 4.51 mmol) and β-hydroxynaphthaldehyde (792 mg, 4.51 mmol). Appearance: Orange color solid. Yield = 87%, 1.95 g. ¹H NMR (500 MHz, CDCl₃, 25 °C): δ (ppm) 15.42 (s, 1H), 9.30 (d, J = 3.50 Hz, 1H), 8.06 (d, J = 8.00 Hz, 1H), 7.78 (d, J = 9.50 Hz, 1H), 7.68 (d, J = 7.50, 1H), 7.63 (d, J = 7.00 Hz, 2H), 7.51 (t, J = 7.25 Hz, 1H), 7.32-7.33 (m, 3H), 7.03 (d, J = 9.50 Hz, 1H), 6.86 (s, 4H), 2.33 (s, 6H), 2.05 (s, 12H). ¹³C NMR (126 MHz, CDCl₃,

25 °C): δ (ppm) 173.1, 153.4, 147.4, 141.7, 140.96, 138.9, 138.5, 137.8, 133.5, 129.6, 128.4, 127.4, 123.9, 119.5, 118.9, 109.0, 23.6, 21.4. ^{11}B NMR (128 MHz, CDCl_3 , 25 °C): δ (ppm) 74.3. ESI-MS, (positive ion mode): calcd for $\text{C}_{35}\text{H}_{34}\text{BNO}$ 495.2733 Da, observed 496.2810 $[\text{M}+\text{H}]^+$.

Synthesis of 3a: Compound **3a** was synthesized following the same procedure used for **1a**. Quantities of the reactants/reagents used and the characterization data as follows: Borylaniline **3b** (535mg, 1.45 mmol) and β -hydroxynaphthaldehyde (279 mg, 1.45 mmol). Appearance: Orange color solid. Yield = 87%, 660 mg. ^1H NMR (500 MHz, CDCl_3 , 25 °C): δ (ppm) 15.55 (s, 1H), 9.26 (s, 1H), 8.06 (d, $J = 8.5$ Hz, 1H), 7.75 (d, $J = 9.0$ Hz, 1H), 7.66 (d, $J = 8.00$, 1H), 7.49 (t, $J = 7.50$ Hz, 1H), 7.30 (t, $J = 7.25$ Hz, 1H), 7.00 (d, $J = 9.50$ Hz, 1H), 6.95 (s, 2H), 6.76 (s, 4H), 2.28 (s, 6H), 2.08 (s, 6H), 2.01 (s, 6H), 2.00 (s, 6H). ^{13}C NMR (126 MHz, CDCl_3 , 25 °C): δ (ppm) 174.1, 152.1, 146.1, 144.0, 142.7, 140.9, 140.6, 139.6, 137.6, 133.7, 129.5, 128.9, 128.9, 128.3, 127.2, 123.8, 123.6, 119.0, 119.0, 108.6, 23.2, 23.0, 23.0, 21.4. ^{11}B NMR (128 MHz, CDCl_3 , 25 °C): δ (ppm) 74.1 ppm. ESI-MS, (positive ion mode): calcd for $\text{C}_{37}\text{H}_{38}\text{BNO}$ 523.3046 Da, observed 524.3125 $[\text{M}+\text{H}]^+$.

Synthesis of 4a:^[51] Compound **4a** was also synthesized following the same procedure used for **1a**. Quantities of the reactants/reagents used and the characterization data as follows: aniline **4b** (0.5 ml, 5.48 mmol) and β -hydroxynaphthaldehyde (943 mg, 5.48 mmol). Appearance: Yellow color solid. Yield = 81%, 1.1 g. ^1H NMR (500 MHz, CDCl_3 , 25 °C): δ (ppm) = 15.47 (s, 1H), 9.26 (s, 1H), 8.04 (d, $J = 8.5$ Hz, 1H), 7.75 (d, $J = 9.00$ Hz, 1H), 7.66 (d, $J = 9.00$, 1H), 7.48 (t, $J = 7.50$ Hz, 1H), 7.43 (t, $J = 7.25$ Hz, 2H), 7.28-7.34 (m, 4H), 7.04 (d, $J = 9.00$ Hz, 1H). ^{13}C NMR (126 MHz, CDCl_3 , 25 °C): δ (ppm) = 171.2, 154.4, 145.0, 137.0, 133.4, 129.8, 129.5, 128.2, 127.4, 126.6, 123.6, 122.6, 120.3, 118.9, 108.8. ESI-MS, (positive ion mode): calcd for $\text{C}_{17}\text{H}_{13}\text{NO}$ 247.0997 Da, observed 248.1076 $[\text{M}+\text{H}]^+$.

Synthesis of 1: To a pre-cooled (0 °C) dichloromethane (10 ml), solution of anil **1a** (100 mg, 0.2 mmol), DIPEA (100 μl , 0.60 mmol) and $\text{BF}_3\cdot\text{OEt}_2$ (70 μl , 0.60 mmol) were added successively. The resulting reaction mixture was warmed to 25 °C and stirring was continued for another 24 hours. The progress of the reaction was monitored by TLC, after the completion of the reaction; the dichloromethane solution was washed with a saturated aqueous sodium bicarbonate solution followed by water (3 X 50 ml). The combined organic layer was dried over anhydrous sodium sulphate and organic volatiles were removed under reduced pressure gave crude product. The product was purified by column chromatography over silica-gel with hexane: ethyl acetate (1:9) mixture as eluent, to furnish the analytically pure compound as a greenish solid. (Yield = 62 %, 68 mg). ^1H NMR (500 MHz, CDCl_3 , 25 °C): δ (ppm) 9.97 (s, 1H), 8.09 (d, $J = 9.00$ Hz, 1H), 7.96 (d, $J = 8.00$ Hz, 1H), 7.84 (d, $J = 8.00$, 1H), 7.62-7.64 (m, 2H), 7.47-7.53 (m, 3H), 7.28 (d, $J = 9.50$ Hz, 1H), 6.84 (s, 4H), 2.30 (s, 6H), 2.04 (s, 12H). ^{13}C NMR (126 MHz, CDCl_3 , 25 °C): δ (ppm) 162.8, 158.4, 147.9, 143.1, 141.1, 141.1, 139.5, 136.9, 130.5, 129.9, 129.6, 129.5, 128.6, 128.2, 127.7, 125.2, 120.7, 119.2, 108.7, 23.7, 21.4. ^{11}B NMR (128 MHz, CDCl_3 , 25 °C): δ (ppm) 0.96 (t, $^1J_{\text{BF}} = 14.12$ Hz, ^{11}B of BF_2), 63.0 (broad, ^{11}B of TAB). ^{19}F NMR (470 MHz, CDCl_3 , 25 °C): δ (ppm) -134.7 (q, $^1J_{\text{FB}} = 11.76$ Hz). ESI-MS, (positive ion mode): calcd for $\text{C}_{35}\text{H}_{33}\text{B}_2\text{F}_2\text{NO}$ 543.2716 Da, observed 566.2616 $[\text{M}+\text{Na}]^+$.

Synthesis of 2: Compound **2** was synthesized following the same procedure described for **1**. Quantities of the reactants/reagents are as follows: Anil (**2a**) (100 mg, 0.20 mmol), $\text{BF}_3\cdot\text{OEt}_2$ (70 μl , 0.60 mmol) and DIPEA (110 μl , 0.60 mmol). Appearance: Orange color solid. Yield = 60%, 65 mg. ^1H NMR (500 MHz, CDCl_3 , 25 °C): δ (ppm) 9.15 (s, 1H), 8.12 (d, $J = 9.00$ Hz, 1H), 8.08 (d, $J = 8.00$ Hz, 1H), 7.86 (d, $J = 8.00$, 1H), 7.64-7.67 (m, 3H), 7.57 (d, $J = 8.00$ Hz, 2H), 7.50-7.51 (m, 1H), 7.30 (d, $J = 9.00$ Hz, 1H), 6.85 (s, 4H), 2.32 (s, 6H), 2.03 (s, 12H). ^{13}C NMR (126 MHz, CDCl_3 , 25 °C): δ (ppm) 163.2, 158.2, 145.5, 141.6, 141.0, 137.7, 131.7, 130.0, 130.0, 128.5, 128.3, 125.4, 123.3, 120.7, 119.4, 109.0. ^{11}B NMR (128 MHz, CDCl_3 , 25 °C): δ (ppm) 1.03 (t, $^1J_{\text{BF}} = 12.84$ Hz, ^{11}B of BF_2), 62.3 (broad, ^{11}B of TAB). ^{19}F NMR (470 MHz, CDCl_3 , 25 °C): δ (ppm) -134.78 (q, $^1J_{\text{FB}} = 10.35$ Hz). ESI-MS, (positive ion mode): calcd for $\text{C}_{35}\text{H}_{33}\text{B}_2\text{F}_2\text{NO}$ 543.2716 Da, observed 566.2614 $[\text{M}+\text{Na}]^+$.

Synthesis of 3: Compound **3** was also synthesized following the same procedure described for **1**. Quantities of the reactants/reagents used and the characterization data as follows: Anil (**3a**) (80 mg, 0.15 mmol), $\text{BF}_3\cdot\text{OEt}_2$ (60 μl , 0.45 mmol) and DIPEA (80 μl , 0.45 mmol). Appearance: Green color solid. Yield = 80%, 70 mg. ^1H NMR (500 MHz, CDCl_3 , 25 °C): δ (ppm) 9.13 (s, 1H), 8.09-8.12 (m, 2H), 7.85 (d, $J = 8.00$ Hz, 1H), 7.65 (t, $J = 7.00$ Hz, 1H), 7.48 (t, $J = 7.50$ Hz, 1H), 7.30 (d, $J = 9.00$ Hz, 1H), 7.16 (s, 2H), 6.77 (s, 4H), 2.28 (s, 6H), 2.11 (s, 6H), 2.01 (s, 12H). ^{13}C NMR (126 MHz, CDCl_3 , 25 °C): δ (ppm) 162.7, 157.6, 143.6, 143.3,

142.4, 141.0, 140.6, 139.9, 131.7, 129.9, 129.6, 129.0, 128.2, 125.2, 122.4, 120.7, 119.4, 108.9, 23.2, 23.1, 21.4. ^{11}B NMR (128 MHz, CDCl_3 , 25 °C): δ (ppm) 0.98 (t, $^1J_{\text{BF}} = 13.61$ Hz, ^{11}B of BF_2), 63.2 (broad, ^{11}B of TAB). ^{19}F NMR (470 MHz, CDCl_3 , 25 °C): δ (ppm) -134.54 (dq, $^2J_{\text{FF}} = 84.00$ Hz, $^1J_{\text{FB}} = 12.00$ Hz, 11.41 Hz), -135.23 (dq, $^2J_{\text{FF}} = 84.00$ Hz, $^1J_{\text{FB}} = 12.00$ Hz, 11.41 Hz). ESI-MS, (positive ion mode): calcd. for $\text{C}_{37}\text{H}_{37}\text{B}_2\text{F}_2\text{NO}$ 571.3029 Da, observed 594.2926 $[\text{M}+\text{Na}]^+$.

For compound **3**, the ^{19}F resonance showed multiple splitting pattern with significantly different chemical shift, which clearly suggests the chemically and magnetically non-equivalent nature of the two fluorine atoms (Figure S23). Each peak for the two fluorine atoms (-134.54 ppm and -135.23 ppm) is splitted into doublet by coupling with the other fluorine ($I = 1/2$) ($^2J_{\text{FF}} = 84.00$ Hz) followed by the splitting of each doublet into quartet ($^1J_{\text{BF}} = 12.00$ Hz and 11.41 Hz) by coupling with quadruple ^{11}B atom ($I = 3/2$). The presence of two methyl group in **3** makes the molecule rigid and is the reason behind the magnetic nonequivalence of fluorine atoms. This type multiple splitting is quite common for BODIPYs where the molecular conformation is locked in some specific conformation.^[59]

Synthesis of 4: Compound **4** was also synthesized following the same procedure described for **1**. Quantities of the reactants/reagents used and the characterization data as follows: Anil (**4a**) 400 mg (1.62 mmol), $\text{BF}_3\cdot\text{OEt}_2$ 60 μl (4.85 mmol) and DIPEA (90 μl , 4.85 mmol). Appearance: Green colour solid. Yield = 220 mg, 46%. ^1H NMR (500 MHz, CDCl_3 , 25 °C): δ (ppm) = 9.12 (s, 1H), 8.12 (d, $J = 9.00$ Hz, 1H), 8.05 (d, $J = 8.50$ Hz, 1H), 7.85 (d, $J = 8.00$, 1H), 7.65 (t, $J = 7.50$ Hz, 1H), 7.61 (d, $J = 8.00$ Hz, 2H), 7.54 (t, $J = 7.50$ Hz, 2H), 7.48-7.51 (m, 2H). ^{13}C NMR (126 MHz, CDCl_3 , 25 °C): δ (ppm) = 162.8, 158.4, 143.0, 141.2, 131.6, 129.9, 129.8, 129.7, 129.2, 128.2, 125.3, 123.8, 120.6, 119.3, 108.8. ^{11}B NMR (128 MHz, CDCl_3 , 25 °C): δ (ppm) = 1.01 (t, $^1J_{\text{BF}} = 13.16$ H), ^{19}F NMR (470 MHz, CDCl_3 , 25 °C): δ (ppm) = -134.55 (q, $^1J_{\text{FB}} = 14.12$ Hz). ESI-MS, (positive ion mode): calcd. for $\text{C}_{17}\text{H}_{12}\text{BF}_2\text{NO}$ 295.0980 Da, observed 318.0876 $[\text{M}+\text{Na}]^+$.

Acknowledgements

P.T, P. S and N. K. K thank Science and Engineering Research Board (SERB), New Delhi, India for financial support. and IISc Bangalore for instrumental facilities. R.P.N. and P.S. thank IISc Bangalore for research fellowship.

Keywords: Triarylborane • Anil • Boranil • Luminescence • Mechanofluorochromism

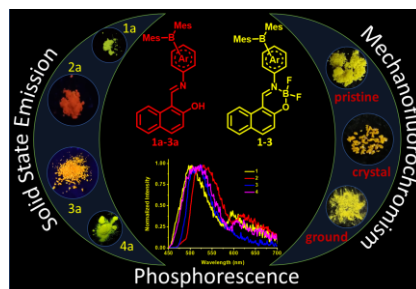
References

- [1] Z. Shen, P. E. Burrows, V. Bulović, S. R. Forrest, M. E. Thompson, *Science* (80-.). **1997**, 276, 2009–2011.
- [2] D. Schneider, T. Rabe, T. Riedl, T. Dobbertin, M. Kröger, E. Becker, H. H. Johannes, W. Kowalsky, T. Weimann, J. Wang, et al., *Adv. Mater.* **2005**, 17, 31–34.
- [3] M. S. Kwon, J. H. Jordahl, A. W. Phillips, K. Chung, S. Lee, J. Gierschner, J. Lahann, J. Kim, *Chem. Sci.* **2016**, 7, 2359–2363.
- [4] A. Kishimura, T. Yamashita, K. Yamaguchi, T. Aida, *Nat. Mater.* **2005**, 4, 546–549.
- [5] S. P. J. T. Bachollet, D. Volz, B. Fiser, S. Münch, F. Röncke, J. Carrillo, H. Adams, U. Schepers, E. Gómez-Bengoa, S. Bräse, et al., *Chem. Eur. J.* **2016**, 22, 12430–12438.
- [6] A. Fukazawa, S. Yamaguchi, *Chem. - An Asian J.* **2009**, 4, 1386–1400.
- [7] D. Li, H. Zhang, Y. Wang, *Chem. Soc. Rev.* **2013**, 42, 8416.
- [8] A. Adamczyk-Woźniak, K. M. Borys, A. Sporzyński, *Chem. Rev.* **2015**, 115, 5224–5247.

- [9] M. Ibarra-Rodríguez, B. M. Muñoz-Flores, H. V. R. Dias, M. Sánchez, A. Gomez-Treviño, R. Santillan, N. Farfán, V. M. Jiménez-Pérez, *J. Org. Chem.* **2017**, *82*, 2375–2385.
- [10] Z. Q. Liu, Q. Fang, D. Wang, D. X. Cao, G. Xue, W. T. Yu, H. Lei, *Chem. Eur. J.* **2003**, *9*, 5074–5084.
- [11] S. Yamaguchi, S. Akiyama, K. Tamao, *J. Am. Chem. Soc.* **2001**, *123*, 11372–11375.
- [12] M. B. Lachachi, T. Benabdallah, P. M. Aguiar, M. H. Youcef, A. C. Whitwood, J. M. Lynam, L. Antonov, W. M. F. Fabian, D. Nedeltcheva, F. S. Kamounah, et al., *J. Am. Chem. Soc.* **2015**, *9*, 281–298.
- [13] T. A. Welsh, A. Laventure, A. F. Alahmadi, G. Zhang, T. Baumgartner, Y. Zou, F. Jäkle, G. C. Welch, *ACS Appl. Energy Mater.* **2019**, *2*, 1229–1240.
- [14] J. Jin, Y. Tao, H. Jiang, R. Chen, G. Xie, Q. Xue, C. Tao, L. Jin, C. Zheng, W. Huang, *Adv. Sci.* **2018**, *5*, DOI 10.1002/adv.201800292.
- [15] S. Griesbeck, E. Michail, C. Wang, H. Ogasawara, S. Lorenzen, L. Gerstner, T. Zang, J. Nitsch, Y. Sato, R. Bertermann, et al., *Chem. Sci.* **2019**, *10*, 5405–5422.
- [16] X. Liu, S. Li, J. Feng, Y. Li, G. Yang, *Chem. Commun.* **2014**, *50*, 2778–2780.
- [17] S. Wang, K. Yuan, M. F. Hu, X. Wang, T. Peng, N. Wang, Q. S. Li, *Angew. Chem. Int. Ed.* **2018**, *57*, 1073–1077.
- [18] C. T. Poon, W. H. Lam, H. L. Wong, V. W. W. Yam, *J. Am. Chem. Soc.* **2010**, *132*, 13992–13993.
- [19] E. Sakuda, A. Funahashi, N. Kitamura, *Inorg. Chem.* **2006**, *45*, 10670–10677.
- [20] A. Nakagawa, A. Ito, E. Sakuda, S. Fujii, N. Kitamura, *Inorg. Chem.* **2018**, *57*, 9055–9066.
- [21] S. Saito, K. Matsuo, S. Yamaguchi, *J. Am. Chem. Soc.* **2012**, *134*, 9130–9133.
- [22] K. Okada, H. Inokawa, T. Sugawa, M. Oda, *J. Chem. Soc. Chem. Commun.* **1992**, 448–449.
- [23] S. Osumi, S. Saito, C. Dou, K. Matsuo, K. Kume, H. Yoshikawa, K. Awaga, S. Yamaguchi, *Chem. Sci.* **2016**, *7*, 219–227.
- [24] V. M. Hertz, M. Bolte, H. W. Lerner, M. Wagner, *Angew. Chem. Int. Ed.* **2015**, *54*, 8800–8804.
- [25] E. von Grothuss, A. John, T. Kaese, M. Wagner, *Asian J. Org. Chem.* **2018**, *7*, 37–53.
- [26] G. R. Kumar, S. K. Behera, P. Thilagar, *Dalton Trans.* **2019**, *48*, 6817–6823.
- [27] S. Pagidi, N. K. Kalluvettukuzhy, P. Thilagar, *Langmuir* **2018**, *34*, 8170–8177.
- [28] D. Frath, J. Massue, G. Ulrich, R. Ziessel, *Angew. Chem. Int. Ed.* **2014**, *53*, 2290–2310.
- [29] J. F. Araneda, W. E. Piers, B. Heyne, M. Parvez, R. McDonald, *Angew. Chem. Int. Ed.* **2011**, *50*, 12214–12217.
- [30] A. Loudet, K. Burgess, *Chem. Rev.* **2007**, *107*, 4891–4932.
- [31] C. A. Swamy P, S. Mukherjee, P. Thilagar, *Chem. Commun.* **2013**, *49*, 993–995.
- [32] S. K. Sarkar, P. Thilagar, *Chem. Commun.* **2013**, *49*, 8558–8560.
- [33] Z. Yan, X. Lin, H. Guo, F. Yang, *Tetrahedron Lett.* **2017**, *58*, 3064–3068.
- [34] S. Shimizu, T. Iino, A. Saeki, S. Seki, N. Kobayashi, *Chem. Eur. J.* **2015**, *21*, 2893–2904.
- [35] Y. L. Rao, C. Hörl, H. Braunschweig, S. Wang, *Angew. Chem. Int. Ed.* **2014**, *53*, 9086–9089.
- [36] D. L. Crossley, I. A. Cade, E. R. Clark, A. Escande, M. J. Humphries, S. M. King, I. Vitorica-Yrezabal, M. J. Ingleson, M. L. Turner, *Chem. Sci.* **2015**, *6*, 5144–5151.
- [37] B. J. Liddle, R. M. Silva, T. J. Morin, F. P. Macedo, R. Shukla, S. V. Lindeman, J. R. Gardinier, *J. Org. Chem.* **2007**, *72*, 5637–5646.
- [38] V. Mukundam, S. Sa, A. Kumari, R. Das, K. Venkatasubbaiah, *J. Mater. Chem. C* **2019**, *7*, 12725–12737.
- [39] D. Kunchala, S. Sa, P. Nayak, J. S. Ponniah, K. Venkatasubbaiah, *Organometallics* **2019**, *38*, 870–878.
- [40] D. Frath, S. Azizi, G. Ulrich, R. Ziessel, *Org. Lett.* **2012**, *14*, 4774–4777.
- [41] A. M. Grabarz, B. Jędrzejewska, A. Zakrzewska, R. Zalesny, A. D. Laurent, D. Jacquemin, B. Ośmiatowski, *J. Org. Chem.* **2017**, *82*, 1529–1537.
- [42] B. Jędrzejewska, A. Skotnicka, A. D. Laurent, M. Pietrzak, D. Jacquemin, B. Ośmiatowski, *J. Org. Chem.* **2018**, *83*, 7779–7788.
- [43] N. Zhao, C. Ma, W. Yang, W. Yin, J. Wei, N. Li, *Chem. Commun.* **2019**, *55*, 8494–8497.
- [44] G. Li, W. Lou, D. Wang, C. Deng, Q. Zhang, *ACS Appl. Mater. Interfaces* **2019**, *11*, 32209–32217.
- [45] K. Dhanunjayarao, V. Mukundam, K. Venkatasubbaiah, *Inorg. Chem.* **2016**, *55*, 11153–11159.
- [46] J. Roßbach, K. Harms, U. Koert, *Org. Lett.* **2015**, *17*, 3122–3125.
- [47] A. Felouat, A. D'Aléo, F. Fages, *J. Org. Chem.* **2013**, *78*, 4446–4455.
- [48] W. A. Morris, T. Liu, C. L. Fraser, *J. Mater. Chem. C* **2015**, *3*, 352–363.
- [49] S. K. Sarkar, G. R. Kumar, P. Thilagar, *Chem. Commun.* **2016**, *52*, 4175–4178.
- [50] S. K. Sarkar, S. Mukherjee, P. Thilagar, *Inorg. Chem.* **2014**, *53*, 2343–2345.
- [51] A. Ohshima, A. Momotake, T. Arai, *J. Photochem. Photobiol. A Chem.* **2004**, *162*, 473–479.
- [52] C. C. Hsieh, C. M. Jiang, P. T. Chou, *Acc. Chem. Res.* **2010**, *43*, 1364–1374.
- [53] B. Li, L. Zhou, H. Cheng, Q. Huang, J. Lan, L. Zhou, J. You, *Chem. Sci.* **2018**, *9*, 1213–1220.
- [54] V. S. Padalkar, S. Seki, *Chem. Soc. Rev.* **2016**, *45*, 169–202.
- [55] L. Ji, R. M. Edkins, L. J. Sewell, A. Beeby, A. S. Batsanov, K. Fucke, M. Drafz, J. A. K. Howard, O. Moutounet, F. Ibersiene, et al., *Chem. Eur. J.* **2014**, *20*, 13618–13635.
- [56] P. Sudhakar, K. K. Neena, P. Thilagar, *J. Mater. Chem. C* **2017**, *5*, 6537–6546.
- [57] P. Sudhakar, S. Mukherjee, P. Thilagar, *Organometallics* **2013**, *32*, 3129–3133.
- [58] S. Yamaguchi, S. Akiyama, K. Tamao, *J. Am. Chem. Soc.* **2000**, *122*, 6335–6336.
- [59] K. K. Neena, P. Thilagar, *Chempluschem* **2016**, *81*, 955–963.
- [60] M. B. Lachachi, T. Benabdallah, P. M. Aguiar, M. H. Youcef, A. C. Whitwood, J. M. Lynam, *Dalton Trans.* **2015**, *44*, 11919–11928.
- [61] X. Jia, J. Nitsch, L. Ji, Z. Wu, A. Friedrich, F. Kerner, M. Moos, C. Lambert, T. B. Marder, *Chem. Eur. J.* **2019**, *25*, 10845–10857.
- [62] A. D. Becke, *Phys. Rev. A* **1988**, *38*, 3098–3100.
- [63] A. D. Becke, *J. Chem. Phys.* **1993**, *98*, 5648–5652.
- [64] C. Lee, W. Yang, R. G. Parr, *Phys. Rev. B* **1988**, *37*, 785–789.
- [65] M. J. Frisch, G. W. Trucks, H. B. Schlegel, G. E. Scuseria, M. A. Robb, et al., Gaussian 09 (Gaussian, Inc., Wallingford CT, **2009**).

- [66] R.D. Dennington, T. A. Keith and J.M. Millam, GaussView 5.0.8, (Gaussian, Inc., Wallingford CT, **2008**).
- [67] J. Seo, S. Kim, S. Y. Park, *J. Am. Chem. Soc.* **2004**, *126*, 11154–11155.
- [68] A. C. Sedgwick, L. Wu, H. H. Han, S. D. Bull, X. P. He, T. D. James, J. L. Sessler, B. Z. Tang, H. Tian, J. Yoon, *Chem. Soc. Rev.* **2018**, *47*, 8842–8880.
- [69] J. E. Kwon, S. Y. Park, *Adv. Mater.* **2011**, *23*, 3615–3642.
- [70] X. Bi, B. Liu, L. McDonald, Y. Pang, *J. Phys. Chem. B* **2017**, *121*, 4981–4986.
- [71] A. Slama-Schwok, M. Blanchard-Desce, J. M. Lehn, *J. Phys. Chem.* **1990**, *94*, 3894–3902.
- [72] J. B. Birks, *Photophysics of Aromatic Molecules*, Wiley, London, **1970**.
- [73] O. Ostroverkhova, *Chem. Rev.* **2016**, *116*, 13279–13412.
- [74] G. Zhou, C. L. Ho, W. Y. Wong, Q. Wang, D. Ma, L. Wang, Z. Lin, T. B. Marder, A. Beeby, *Adv. Funct. Mater.* **2008**, *18*, 499–511.
- [75] Z. M. Hudson, C. Sun, M. G. Helander, Y. L. Chang, Z. H. Lu, S. Wang, *J. Am. Chem. Soc.* **2012**, *134*, 13930–13933.
- [76] X. Wang, Y. L. Chang, J. S. Lu, T. Zhang, Z. H. Lu, S. Wang, *Adv. Funct. Mater.* **2014**, *24*, 1911–1927.
- [77] T. Kushida, C. Camacho, A. Shuto, S. Irle, M. Muramatsu, T. Katayama, S. Ito, Y. Nagasawa, H. Miyasaka, E. Sakuda, et al., *Chem. Sci.* **2014**, *5*, 1296–1304.
- [78] G. Zhang, J. Chen, S. J. Payne, S. E. Kooi, J. N. Demas, C. L. Fraser, *J. Am. Chem. Soc.* **2007**, *129*, 8942–8943.
- [79] Z. Yang, Z. Mao, X. Zhang, D. Ou, Y. Mu, Y. Zhang, C. Zhao, S. Liu, Z. Chi, J. Xu, et al., *Angew. Chem. Int. Ed.* **2016**, *55*, 2181–2185.
- [80] W. R. Dawson, M. W. Windsor, *J. Phys. Chem.* **1968**, *72*, 3251–3260.
- [81] APEX2 (Version 2008.1-0). Bruker AXS Inc.: Madison, Wisconsin, USA **2008**.
- [82] SAINT-NT, Version 6.04; Bruker AXS. Madison, Wisconsin, USA **2001**.
- [83] G. M. Sheldrick, "SADABS, Software for Empirical Absorption Corrections,," University of Göttingen, Göttingen **1996**.
- [84] G. M. Sheldrick, *Acta Crystallogr. Sect. A Found. Crystallogr.* **2008**, *64*, 112–122.
- [85] L. J. Farrugia, *J. Appl. Crystallogr.* **1999**, *32*, 837–838.
- [86] P. van der Sluis, A. L. Spek, *Acta Crystallogr. Sect. A Found. Crystallogr.* **1990**, *46*, 194–201.

Entry for the Table of Contents



Effect of incorporation of electron deficient triarylboron on the optical properties of anils and boranils are rationalized with a series of triarylborane coupled anils and boranils. The nature of the spacer and the position of TAB on the spacer have an effect on the properties of these compounds. All the compounds are emissive in solid state and exhibit stimuli responsive mechanofluorochromism property and phosphorescence at low temperature.